Soft Matter

Polymerization in Soft Nanoconfinements of Lamellar and Reverse Hexagonal Mesophases

Journal:	*Soft Matter*
Manuscript ID	SM-ART-08-2019-001565.R1
Article Type:	Paper
Date Submitted by the Author:	07-Sep-2019
Complete List of Authors:	Qavi, Sahar; New Mexico State University, Chemical and Materials Engineering Bandegi , Alireza; New Mexico State University, Chemical and Materials Engineering Firestone, Millicent; Los Alamos National Laboratory, Materials Physics & Applications Foudazi, Reza; New Mexico State University, Chemical and Materials Engineering

Polymerization in Soft Nanoconfinements of Lamellar and Reverse Hexagonal Mesophases

Sahar Qavi[1], Alireza Bandegi[1], Millicent Firestone[2], Reza Foudazi[1*]

[*] Corresponding author, Email: rfoudazi@nmsu.edu.

[1]Department of Chemical and Materials Engineering, New Mexico State University, Las Cruces, NM 88003

[2]Materials Physics & Applications Division, Center for Integrated Nanotechnologies, Los Alamos National Laboratory

Abstract

This work describes the kinetics of thermal polymerization in nanoconfined domains of lyotropic liquid crystal (LLC) templates by using chemorheological studies at different temperatures. We investigate lamellar and reverse hexagonal LLC phases with the same concentration of monomeric phase. Results show that the mesophase structures remain intact during thermal polymerization with very slight changes in the domain size. The polymerization rate decreases in the nanoconfined structure compared to the bulk state due to the segregation effect that increases the local monomer concentration and enhances the termination rate. Additionally, the polymerization rate is faster in the studied reverse hexagonal systems compared to the lamellar ones due to their lower degree of confinement. A higher degree of confinement also induces a lower monomer conversion. Differential scanning calorimetry confirms the obtained results from chemorheology.

Introduction

Self-assembly of amphiphilic molecules in the presence of two solvents (oil/water) leads to the formation of lyotropic liquid crystals (LLCs) with the length scale in the range of 2-50 nm, also called mesophases. Direct templating by preformed LLC phases has widely been used for producing organic and inorganic mesoporous materials.[1–7] For making

organic mesoporous media, after preparation of oil/water/surfactant in a desired phase state, one of the phases can be polymerized to obtain a mesoporous polymer. Thus, monomers are included in the oil or water phase prior to the preparation of mesophase. In such cases, we deal with polymerization in nanoconfinement. However, templating method for making organic porous polymers is not a straightforward task. In other words, phase separation during polymerization may change the original nanostructure in terms of shape and size.[8–13] Studying the kinetics of polymerization in nanoconfinement helps in understanding the effect of different types of confinement on the final polymer properties.[14]

Several studies have been done on the kinetics of polymerization in hard nanoconfinements.[15–19] At the early stages of polymerization in the anodic aluminum oxide templates, it has been observed that the template walls catalyze the initiation reaction and the polymerization rate increases. However, at the late stages of polymerization, the termination reaction increases as the likelihood of radicals being in the close proximity increases, which leads to the lower conversion and reaction rate.[15] Confinement is one of the main factors contributing to the polymerization rate. As the system is more confined, the local monomer concentration increases, which leads to higher termination rate and lower polymerization rate.[15] Figure 1a schematically shows the effect of confinement.

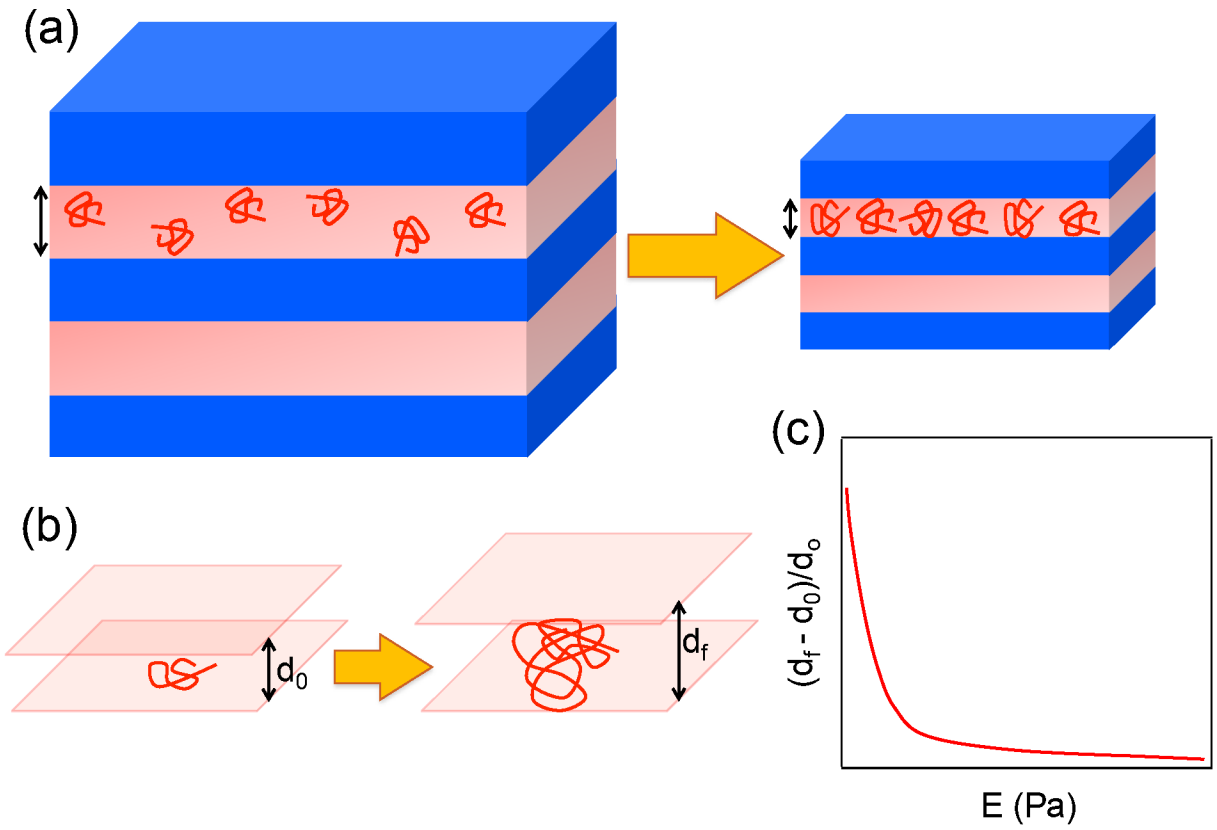

Figure 1.Schematic illustration of: (a) the effect of confinement on the probability of termination reactions, (b) the increase in domain size upon polymerization due to the tendency of polymer chains to form random coil, and (c) the expected dependence of change in domain size upon polymerization to the template modulus (see eq. 1).

In soft nanoconfinements, the template stiffness also plays a role in the polymerization kinetics. Therefore, the degree of confinement, as the prominent factor affecting the polymerization kinetics, is influenced by the size of the confinement and the template stiffness. In other words, as the degree of polymerization increases, polymer chains tend towards random coil conformation to minimize their free energy (Figure 1b). If the template stiffness cannot suppress the tendency of the random coil conformation, the domain size will increase. In an ideal case, the higher the elastic modulus of a soft template, the lower is the change in the domain size upon polymerization, thus, the higher is the effect of confinement at a fixed initial domain size (Figure 1c). Hard templates can be considered to have very large modulus with no change in the domain size, whereas a

template with zero modulus will be destroyed upon polymerization (maximum change in domain size). Assuming negligible density change during polymerization, therefore, we can propose the following scaling relationship:

$$\frac{d_f - d_0}{d_0} \propto \frac{1}{E^n} \quad (1)$$

where d_f and d_0 are the final and initial domain sizes, E is the elastic modulus, and n has a value equal or higher than unity. A deviation from this scaling suggests that properties of the template (e.g., surface tension) change during polymerization and extra care should be taken to consider the elastic modulus or change in the domain size as a measure of template stiffness.

Kinetics of photopolymerization in the hexagonal and lamellar mesophases formed with small molecule surfactants have been studied via differential scanning calorimetry (DSC). However, the obtained structures from such mesophases after polymerization have usually a domain size bigger than 100 nm,[20] and/or have been disrupted due to the polymerization-induced phase separation.[20,21] Lester et al.[2] have shown that reactions in the ordered structure of LLCs are highly dependent on the type and degree of order, and are significantly different from the isotropic state. This phenomenon can be attributed to a number of factors including diffusional limitation which reduces termination rates and the segregation of the monomeric species that increases both the apparent propagation and termination rates.[20,22,23] It has been shown that the rate of polymerization and mesophase structure play important roles in the final properties of resulting polymer.[23] Lester et al. observed that for the lyotropic lamellar mesophases made from fluorinated amphiphilic monomers, the termination rate decreases and the polymerization rate increases. Cubic structures, on the other hand, show the slowest kinetics.[23] In another work, they have shown that the polymerization rate of hydrophobic monomers is higher in the micellar cubic structures compared to the lamellar and hexagonal phases. They attributed this behavior to the increase in the rate of propagation in the cubic micelles due to higher local monomer concentration as compared to the other systems.[2]

Pluronic block copolymers are amphiphilic molecules that are widely used as surfactants.[24–27] Photopolymerization of hydrophilic and hydrophobic monomers in LLC

structures formed by Pluronic L92 has been studied.[28] It has been found that the rate of polymerization of hydrophobic monomers in normal phases increases due to the segregation of monomers during photopolymerization. On the other hand, it has been observed that for hydrophilic monomers, the polymerization rate is higher in the inverse phases, such as inverse hexagonal. These results show that the monomer segregation into confined domains of LLCs affects the polymerization rate due to the increases in the local concentration of monomers and/or radicals. Additionally, Lester et al. observed that the diffusion of propagating sites will be limited in confinement.[29]

Zhao et al.[16] have studied the polymerization of methyl methacrylate in hard nanopores and found that smaller pore sizes result in shorter autoacceleration times. They have also shown that hydrophilic pores have a more significant effect in reducing the polymerization activation energy compared to the hydrophobic ones. Silies et al.[30] compared the polymerization rate of zwitterionic monomers inside and on the outer surface of a mesoporous film. They showed that the confinement in mesopores limits the diffusion of monomers and free radicals into the pores and influences the termination rate.

Thermal polymerization is favored over photopolymerization for large-scale production of mesoporous structures. However, there are only few studies addressing the kinetics of thermal polymerization in different mesophases.[31,32] DePierro et al.[10] have compared the structures resulting from photo and thermal polymerizations of acrylamide mixtures in different mesophases formed from small molecule surfactants. They have found that thermal polymerization yields less ordered to disordered structures with larger feature sizes due to the slower kinetics of polymerization.

While chemorheology has been used for studying the kinetics of polymerization for decades,[33–36] only a few studies have been done on chemorheology in nanoconfinements. Peng et al.[37] have studied the photopolymerization of a polymerizable surfactant in binary mixtures of water and Brij 97 in order to maintain the structure upon curing. They have measured the change in the mechanical properties during photopolymerization using *in situ* photo-rheology and found out that the dynamic moduli and viscosity of polymerizing system increase upon exposure to UV light. However, they have not quantified the kinetics of polymerization using rheology. Chow et al.[38,39] have

studied the chemorheology of rod-like poly(p-phenylenebenzobisthiazole) made by polycondensation reactions. They have observed that when the polymer mixture becomes isotropic, the polymerization rate increases as alignment of rods facilitates the condensation reaction.

Recently, we have shown that mesophases of Pluronic/water/monomer with lamellar and hexagonal structures can retain their mesostructure upon thermal polymerization.[40] In this paper, we study the rheological behavior of mesophases during polymerization. Mesophases with the same amount of monomer phase but different structures are used to cancel the effect of monomer and initiator concentration on the polymerization rate. DSC is used to confirm the kinetics of polymerization derived from chemorheology.

Experimental

Pluronic block copolymers, P84 (M_w=4200 g/mol), L121 (M_w=4400 g/mol), and L64 (M_w=2900 g/mol) are kindly provided by BASF. Butyl acrylate (≥99%, Sigma-Aldrich) and ethylene glycol dimethcrylate (EGDMA, purified, Electron Microscopy Sciences) are used as monomer and crosslinker, respectively. Azobisisobutyronitrile (AIBN, 98%, Sigma-Aldrich) is used as the thermal initiator. Deionized (DI) water (0.055 μs/cm, EMD Millipore Direct-Q3) is used as the aqueous phase. The monomer and crosslinker are purified by passing through a silica column. All other chemicals are used as received without further purification.

Method of mesophase preparation has been explained before.[40] Simply, desired amounts of components are mixed using centrifugation at alternative direction until a transparent mesophase is obtained. Table 1 shows the ratio of materials used in each sample. The monomer to crosslinker weight ratio is held constant at 3:1 and the initiator concentration is 3 wt% of the monomer in all samples. Samples are formulated in a way that the monomer plus crosslinker concentration is constant, but different mesostructures are made by varying water/block copolymer ratio. It should be noted that it is almost impossible to have different mesostructures with the same Pluronic at a fixed oil phase (monomer) concentration. Thus, we have used different Pluronic block copolymers while

keeping the concentration of the polymerizing phase at 25 wt%. We prepare two lamellar, L_α, mesophases with P84/water/monomers 60/15/25 wt% and L121/water/monomers 57/18/25 wt%, and two inverse hexagonal, H_2, mesophases with P84/water/monomers 40/35/25 wt% and L64/water/monomers 55/20/25 wt%.

Small angle X-ray scattering (SAXS) is used to confirm the mesostructure of each sample. Measurements use Cu Kα X-rays radiation source with the wavelength of 1.54184 Å using Bruker Nanostar System. All samples are tested before and after polymerization to ensure desired mesophases are made and samples retained their structures upon polymerization.

A stress-controlled rheometer DHR-3 (TA Instruments, New Castle, DE) is used to study the rheological behavior and chemorheology of mesophases. A 40 mm sand blasted parallel plate geometry with 1 mm gap is used in all experiments. All tests are performed in the linear viscoelastic region (0.5% strain, confirmed from amplitude sweep tests). First, dynamic frequency sweep tests are performed at 25 °C in the frequency range of 0.1 to 600 rad/s. For chemorheology studies, a solvent trap filled with DI water is used. Time tests in small amplitude oscillatory shear mode are done on mesophases at three different temperatures, 60, 65, and 70°C to determine the kinetics of polymerization through evolution of elastic and loss moduli.[33] Data are collected in the linear viscoelastic region (strain amplitude of 0.5%) at constant frequency of 1 Hz. Polymerization of the pure monomer phase, consist of butyl acrylate, EGDMA (33 wt% of butyl acrylate), and AIBN (3 wt% of butyl acrylate) is also studied as the control sample to define the kinetics of polymerization in the non-confined state.

Isothermal DSC is carried out utilizing Q2000 (TA Instruments, New Castle, DE). Approximately 10 mg of mesophase is placed in the aluminum pans and the heat of reaction is recorded with time. All measurements are performed under a nitrogen gas atmosphere at elevated temperatures (60, 65, and 70 °C) to determine the rate of polymerization according to the procedure established by Guymon and coworkers.[1,2,21,22] Having the heat flow, ΔQ, the polymerization rate, R_p, can be calculated as:

$$\frac{R_p}{[M]_0} = \Delta Q\left[\left(\frac{M_W}{n\Delta H_p m}\right)_{monomer} + \left(\frac{M_W}{n\Delta H_p m}\right)_{crosslinker}\right] \quad (2)$$

where M_w, $[M]_0$, ΔH, n, and m are molecular weight, initial concentration, theoretical reaction enthalpy (86,200 J/mol for acrylate and 56,000 J/mol for methacrylate),[41] functionality, and mass, respectively.[20] Polymerization of pure oil phase is also studied as control sample to define the kinetics of polymerization in the non-confined state. The polymerization rate is normalized to the total reactive species' concentration in the formulation. The reaction temperature is maintained constant (within ± 0.1 °C) during the measurements. The degree of monomer conversion is calculated by integrating the area between the DSC curves and the baseline established by extrapolation from the trace produced after complete polymerization. The final conversion is experimentally obtained by washing the mesophases with soxhlet to remove residual monomer, initiator, and crosslinker. There is also a possibility of block copolymer removal during washing. Samples are first washed with water for 12 h, and then with methanol for another 24 h. Thermal gravimetric analysis (TGA) is done on the washing solvents after soxhlet to confirm that Pluronic block copolymer has not been washed out, as shown in Figure S1 in the Electronic Supplementary Information (ESI). After washing, the samples are dried in the vacuum oven at 40 °C for 48 h. Dried samples are weighed and the conversion is obtained using the gravimetric analysis.

Results and discussion

SAXS

To confirm the retention of mesostructures upon thermal polymerization, SAXS studies are done on the mesophases before and after polymerization as shown in Figure 2.

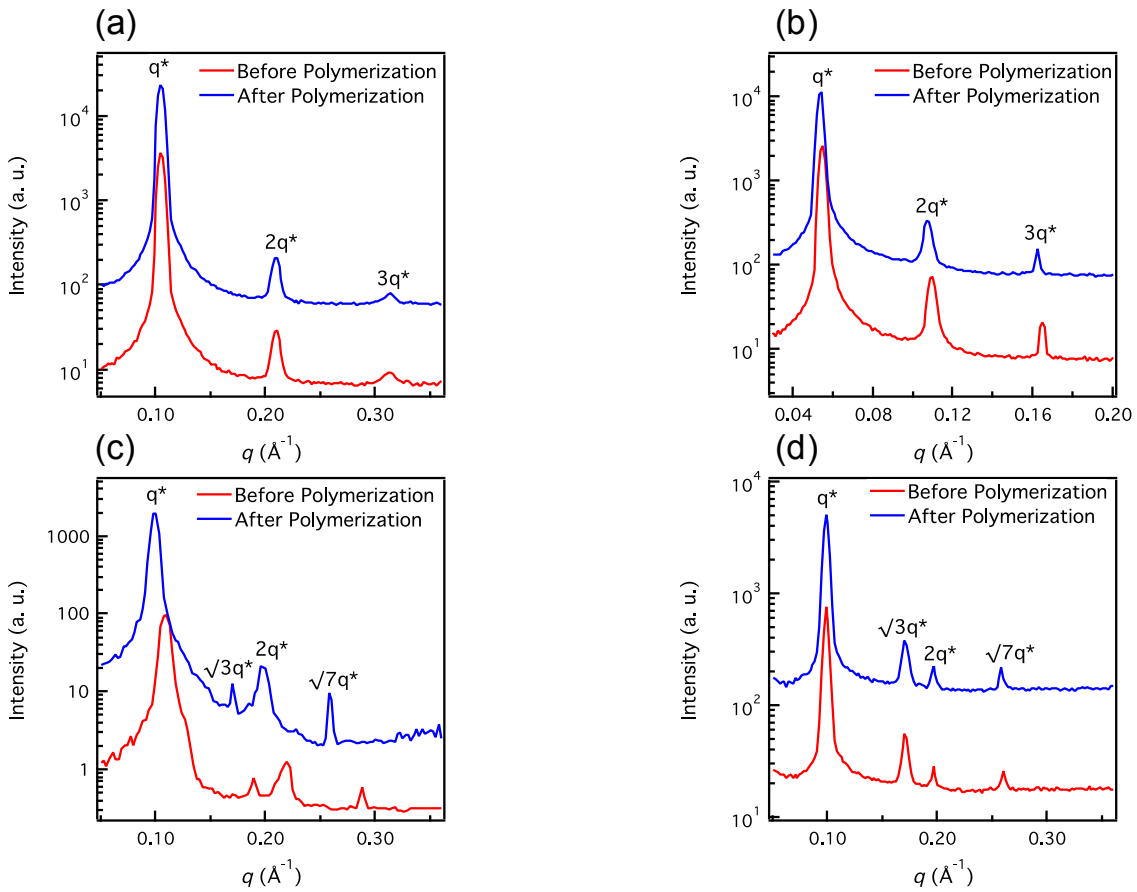

Figure 2. 1D SAXS graphs of mesophase systems with different Pluronic block copolymer/water/oil (wt%) compositions before and after polymerization: (a) P84-L_α (60/15/25), (b) L121-L_α (57/18/25), (c) P84-H_2 (40/35/25), and (d) L64-H_2 (55/20/25). Oil phase consists of butyl acrylate, EGDMA, and AIBN.

Lamellar structures have 1:2:3:4:… relative positions of Bragg peaks (q/q*), while hexagonal mesostructures have 1:√3:2:√7:… relative positions of Bragg peaks, where q* is the principal peak. Polymerized samples at elevated temperatures show the same pattern in the peak positions, while there is a slight shift of peaks to the left. According to Bragg's equation, in the lamellar mesophases, lattice parameter, d, can be calculated as:[42]

$$d = \frac{2\pi}{q^*} \quad (3)$$

Apolar domain volume fraction, ϕ, is defined as the volume fraction of the polymerizing phase and the PPO block, and the polar domain volume fraction, $1-\phi$, is the volume

fraction of the water and the PEO block. Knowing the lattice parameter and the volume fractions, we can calculate the lamellar apolar domain size, δ, as:

$$\delta = \phi d \quad (4)$$

In case of hexagonal mesophases, lattice parameter, a, and apolar domain size, α, are calculated as follows:

$$\mathrm{a} = \frac{4\pi}{\sqrt{3}q^*} \quad (5)$$

$$\alpha = \mathrm{a}\left(\frac{\sqrt{3}}{2\pi}\phi\right)^{1/2} \quad (6)$$

In all the above calculations, we assume that different phases of water, oil, PEO, and PPO are completely segregated and the bulk density of each component is considered.[40,42] This assumption might not be accurate as both PEO and PPO partially segregate in water and oil, respectively and EGDMA may have a tendency towards water phase. However, the assumption helps with simplifying the calculations without losing a great deal of information. [40,43] The calculated parameters obtained from SAXS experiments on various samples are schematically shown in Figure 3 and their values are summarized in Table 1. Apolar domain size and its change after polymerization are two important factors in the kinetics of polymerization and will be discussed later.

Critical molecular weight entanglement (M_c) for polyethylene oxide (PEO) and polypropylene oxide (PPO) are 10,000 g/mol and 7,000 g/mol, respectively.[44,45] All the Pluronic block copolymers in our study have the molecular weight well below M_c. Therefore, block copolymers are not entangled in the system. Additionally, the radius of gyration of Pluronic P84, Pluronic L121, and Pluronic L64 block copolymer are approximately 17 Å,[25] 18 Å,[46] and 19 Å,[47] respectively, which are smaller than the domain size of the micelles. Thus, there is no chain crossing the oil phase from one hydrophilic domain to another one.

Table 1. Composition of the samples and their calculated SAXS parameters.

Sample	Pluronic/water/ monomers (wt%)	ϕ	d or a, unpolymerized (nm)	δ or α, unpolymerized (nm)	Intermicellar distance (nm)
P84- L_α	60/15/25	0.62	6.0	3.7	0.9
L121-L_α	57/18/25	0.31	10.0	3.1	1.6
P84- H_2	40/35/25	0.50	6.6	2.4	0.6
L64-H_2	55/20/25	0.60	7.4	3.0	0.8

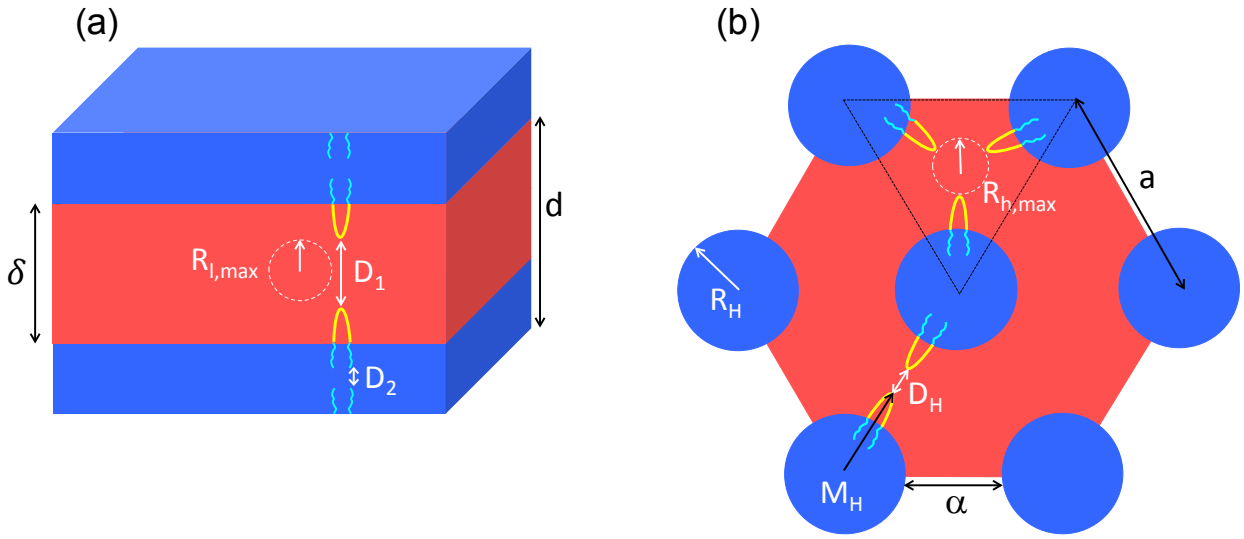

Figure 3. Schematic illustration of the parameters obtained from SAXS and confinement size in (a) lamellar and (b) reverse hexagonal mesophases.

The polymerized samples show a slight shift in the peaks to smaller scattering vectors, which indicates an increase in the lattice parameter, thus, in the apolar domain size. The change in domain size is attributed to the competition between thermodynamics and kinetics. By progression of polymerization, the molecular weight and degree of polymerization, N, increase, thus, the enthalpic penalty, χN, outweighs the entropic contribution to the Gibbs free energy. Therefore, the system is driven towards the increase in domain size (and ultimately phase separation). On the other hand, the density of the monomer phase increases upon polymerization ($\Delta\rho{\sim}10\%$), which leads to the shrinkage and decrease in the domain size. The presence of Pluronic block copolymers with slow dynamics decreases the rate of phase separation. In addition, crosslinking arrests and preserves the structure during thermal polymerization.

Rheology

Amplitude sweep test is done on samples at different temperatures (25, 35, and 45°C) and frequencies (1, 10, and 100 rad/s) to verify the linear viscoelastic region. Data are shown in Figures S2-S9 in the ESI, where we conclude that all samples are in the linear regime at 0.5% strain. The real-time monitoring of stress and strain signals by time also confirms the linear behavior during the polymerization (i.e., the waves remain sinusoidal). Frequency sweep results for lamellar and reverse hexagonal mesophases in Figure 4 show that all mesophases have solid-like behavior, where the elastic modulus is higher than the loss modulus in the studied range of frequency.[48] Such behavior has been observed for suspensions, block copolymer solutions, and highly concentrated emulsions.[49–51] In the systems under study, the solid-like behavior is due to the high concentration of block copolymer and the compact LLC structures. It has been shown that lamellar structures have one order of magnitude lower elastic modulus (G') when compared with hexagonal mesophases.[52,53] As it is evident from Figure 4, the elastic modulus in (c) and (d) plots (H_2 samples) is higher than that of (a) and (b) ones (L_α samples). Comparing the lamellar samples, P84-L_α (60/15/25) shows higher elastic modulus compared to L121-L_α (57/18/25), which is due to the smaller domain size and intermicellar distance in P84-L_α sample. According to a model we have developed recently on the basis of van der Waals interactions (which is the main source of intermicellar interactions),[43] the elastic modulus is highly dependent on the reciprocal of intermicellar distance. There are two intermicellar distances D_1 and D_2 across the oil phase and water phase in the lamellar mesophases, respectively (see Figure 3). Considering that the van der Waals forces between planes scale with D^{-3},[54] an average intermicellar distance in the lamellar systems, D_L, can be defined as follows:

$$\frac{1}{{D_L}^3} = \frac{1}{{D_1}^3} + \frac{1}{{D_2}^3} \quad (7a)$$

$$D_1 = \varphi_{oil} d \quad (7b)$$

$$D_2 = \varphi_{water} d \quad (7c)$$

where φ_{oil} and φ_{water} are the volume fractions of oil and water, respectively. Average intermicellar distance in P84-L_α sample is smaller than that of L121-L_α sample and consequently the elastic modulus is higher in P84-L_α sample.

Additionally, in the reverse hexagonal mesophases, P84-H_2 (40/35/25) has higher elastic modulus than L64-H_2 (55/20/25). Intermicellar distance in reverse hexagonal systems, D_H , can be defined as follows:[43]

$$D_H = \mathrm{a} - 2M_H \quad (8a)$$

$$M_H = \mathrm{a}\sqrt{\frac{\sqrt{3}}{2\pi}(\varphi_{Pluronic} + \varphi_{water})} \quad (8b)$$

where $\varphi_{Pluronic}$ is the volume fraction of Pluronic block copolymer. The intermicellar distance in P84-H_2 sample is smaller than that of L64-H_2 sample. Thus, the elastic modulus is higher in P84-H_2 sample.[43]

A shallow minimum is observed in the loss modulus (G'') curves of all samples that is the characteristic of polymeric gels and has been observed for emulsions and soft-glassy materials as well.[55–59] The minimum in the loss modulus shows the presence of two relaxation behaviors in the system and the transition from α-relaxation observed in low frequencies (long time, related to large domain sizes, i.e., grain size scale) to β-relaxation observed in high frequencies, (>10^3 rad/s), (short time, related to small domain sizes, i.e., micelle size scale).[60] We have recently shown that the higher is the probability of finding defects in the LLC systems, the higher is the angular frequency where the minimum in G'' takes place.[60]

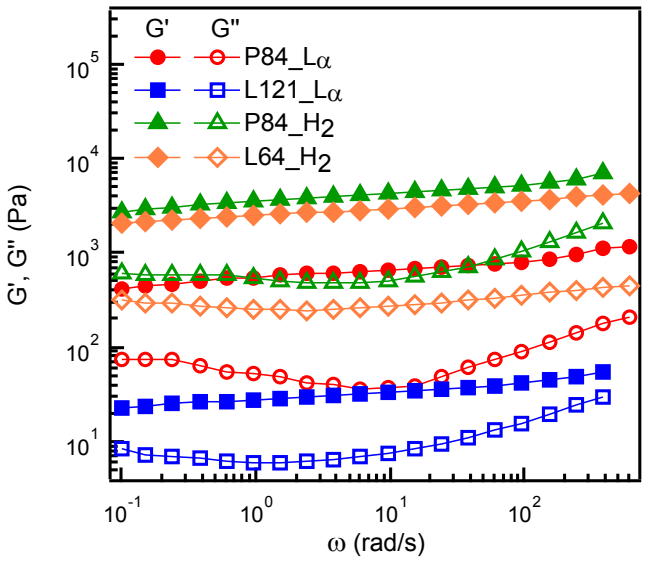

Figure 4. Frequency sweep curves of mesophase systems with different Pluronic block copolymer/water/oil (wt%) compositions: P84-L_α (60/15/25), L121-L_α (57/18/25), P84-H_2 (40/35/25), and L64-H_2 (55/20/25).

Variations of the dynamic moduli with time at three different temperatures for the lamellar and reverse hexagonal samples are shown in Figure 5. Bulk data are provided in Figure 6a. Three stages of polymerization can be found: (i) induction, where G' is relatively constant in the beginning of the experiment for a period indicated as t_{in}; (ii) polymerization, where G' sharply increases by time; and (iii) final curing and end of reaction, where G' reaches a plateau.

Gel point terminology in the conventional chemorheology literature cannot be applied here because of the solid-like behavior of the samples (see Figure 3).[61] Additionally, the G'=G" or tan δ=1 criterion[62] cannot be used as no crossover between dynamic moduli is observed. Considering the gel point as the time when G" is maximum does not work either since G" does not show a maximum in the samples under study.[33,62,63] Therefore, evolution of dynamic moduli and complex viscosity are fitted using Arrhenius type models to determine the kinetic constants.[64]

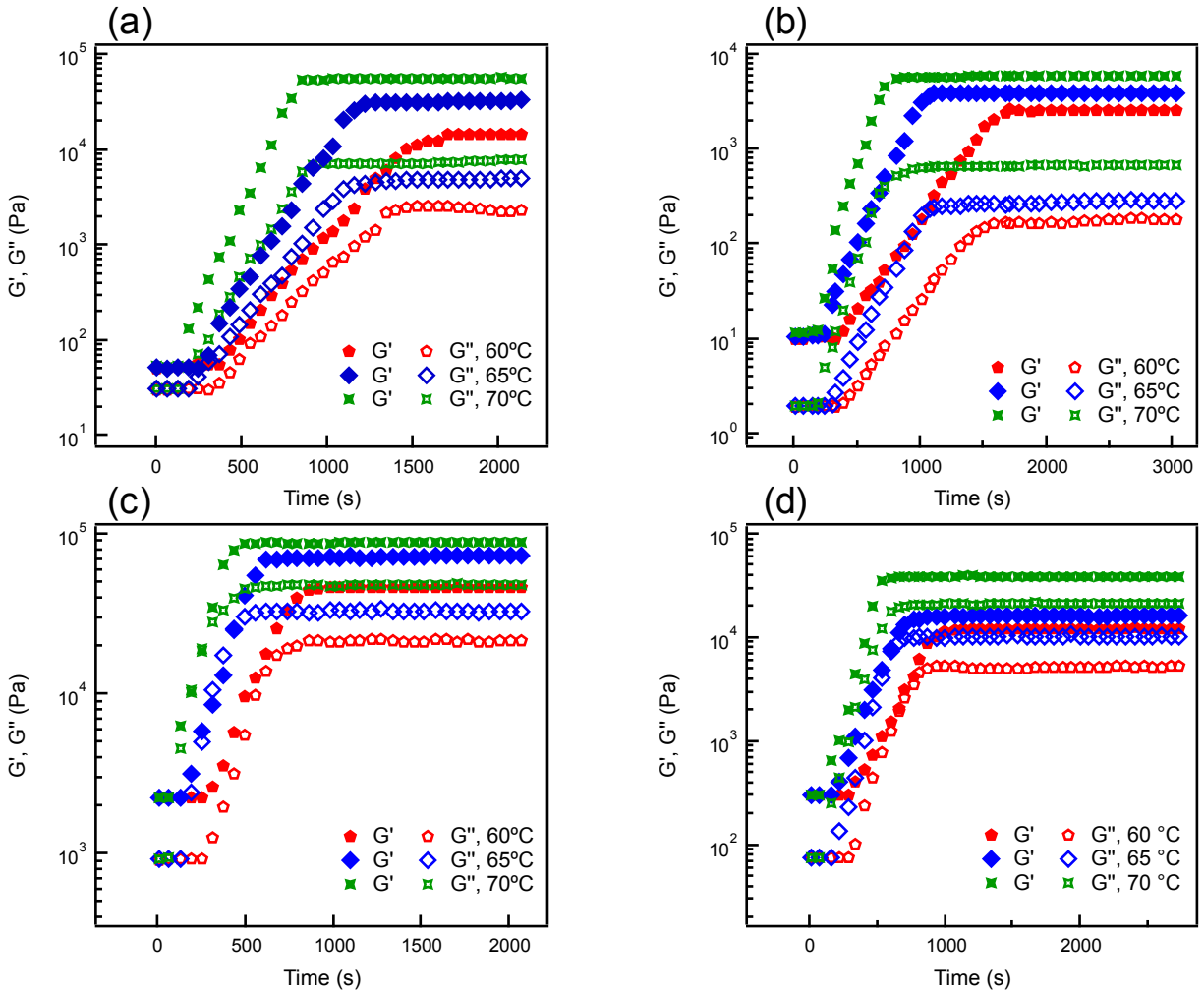

Figure 5. Variation of dynamic moduli with time at three different temperatures (60, 65, and 70 °C) for (a) P84-L_α, (b) L121-L_α, (c) P84-H_2, and (d) L64-H_2 samples.

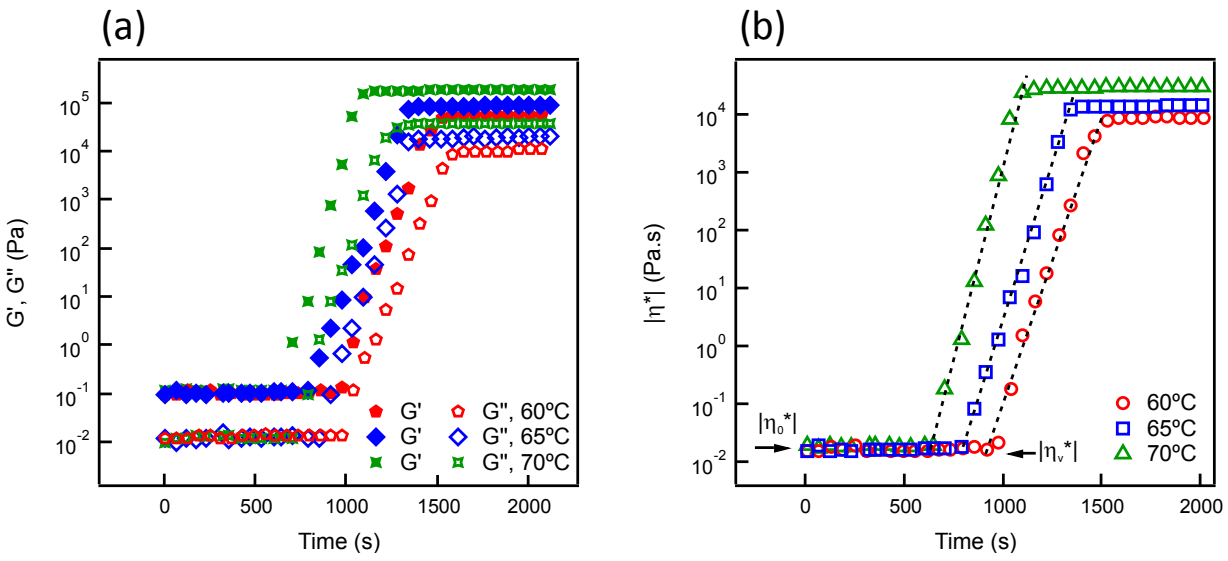

Figure 6. Variation of (a) dynamic moduli and (b) complex viscosity with time at three different temperatures (60, 65, and 70 °C) for bulk sample.

Activation energy in the induction step can be modeled using the Arrhenius model as follows for the induction time, t_{in}:[33]

$$t_{in} = \mathrm{A}\, e^{\left(\frac{E_{in}}{RT}\right)} \tag{9}$$

where E_{in}, R, T, and A are the induction activation energy, gas constant, absolute temperature, and the pre-exponential factor, respectively. Having t_{in} at different temperatures, we can calculate the activation energy from the slope of $\ln t_{in}$ versus $\frac{1}{RT}$ graph (Figure 6).

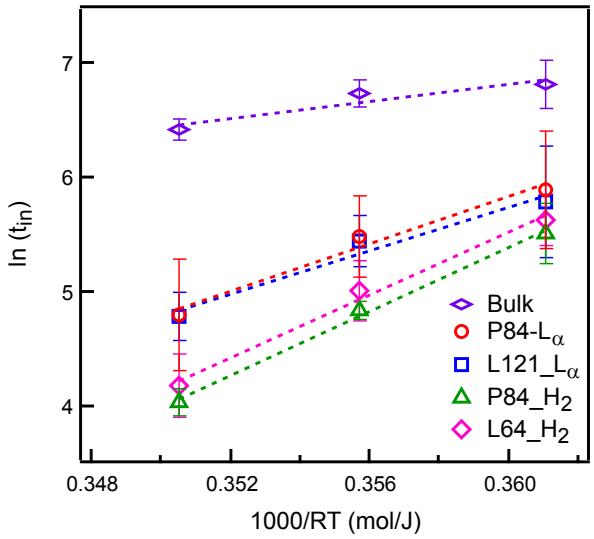

Figure 7. The effect of temperature on the induction time of the polymerization in bulk sample and mesophases of P84-L_α, L121-L_α, P84-H_2, and L64-H_2. The slopes of the lines are used to estimate the induction activation energy.

The values of the induction activation energy for different samples are shown in Table 2. The activation energies for confined samples are higher than the bulk sample that is due to the higher viscosity of confined mesophases that influences the diffusion-controlled initiation in the systems. The lamellar samples show slightly lower induction activation energy compared to the reverse hexagonal ones because of their lower viscosity as confirmed from rheology. It should be noted that having a relatively large uncertainty in the induction times of the lamellar and reverse hexagonal mesophases (Figure 7), caution should be taken when comparing the activation energies of these two systems.

To calculate the polymerization rate, the evolution of LLC complex viscosity, $|\eta^*|$, during polymerization (Figure 8) is used. The first order double Arrhenius model is used to describe the chemorheological data:[33,64]

$$\ln|\eta^*| = \ln|\eta^*_v| + \frac{E_v}{RT} + tK \quad (10)$$

where $|\eta^*_v|$ is the initial complex viscosity before polymerization, and E_v is the viscous activation energy. K is the polymerization rate constant, which is related to the curing temperature as:

$$K = k_0 \exp\left(\frac{-E_p}{RT}\right) \quad (11)$$

where E_p is the activation energy of polymerization.

Table 2. Model parameters for the induction and propagation steps of polymerization in the bulk, lamellar and reverse hexagonal samples.

Sample	T (°C)	E_{in} (kJ/mol)	K (10^{-3}/s)	E_p (kJ/mol)	Confinement size (nm)	Change in apolar domain size (%)	Complex viscosity (Pa.s) at ω=1 Hz
Bulk	60	38±11	21.6±1.1	38.4±0.7	NA	NA	NA
	65		24.1±1.0				
	70		32.4±1.4				
P84- L_α	60	104±12	4.7±0.2	64.8±2.1	0.8	0.12	9.55
	65		6.5±0.3				
	70		9.3±0.2				
L121-L_α	60	96±27	4.6±0.1	67±0.1	1.2	1.85	1.86
	65		7.2±0.4				
	70		9.4±0.2				
P84- H_2	60	141±13	5.4±0.3	74.4±3	1.3	11.02	384.86
	65		8.5±0.1				
	70		11.8±0.3				
L64-H_2	60	138±6	5.5±0.2	69.4±1.8	1.5	0.09	49.93
	65		8.0±0.1				
	70		11.2±0.2				

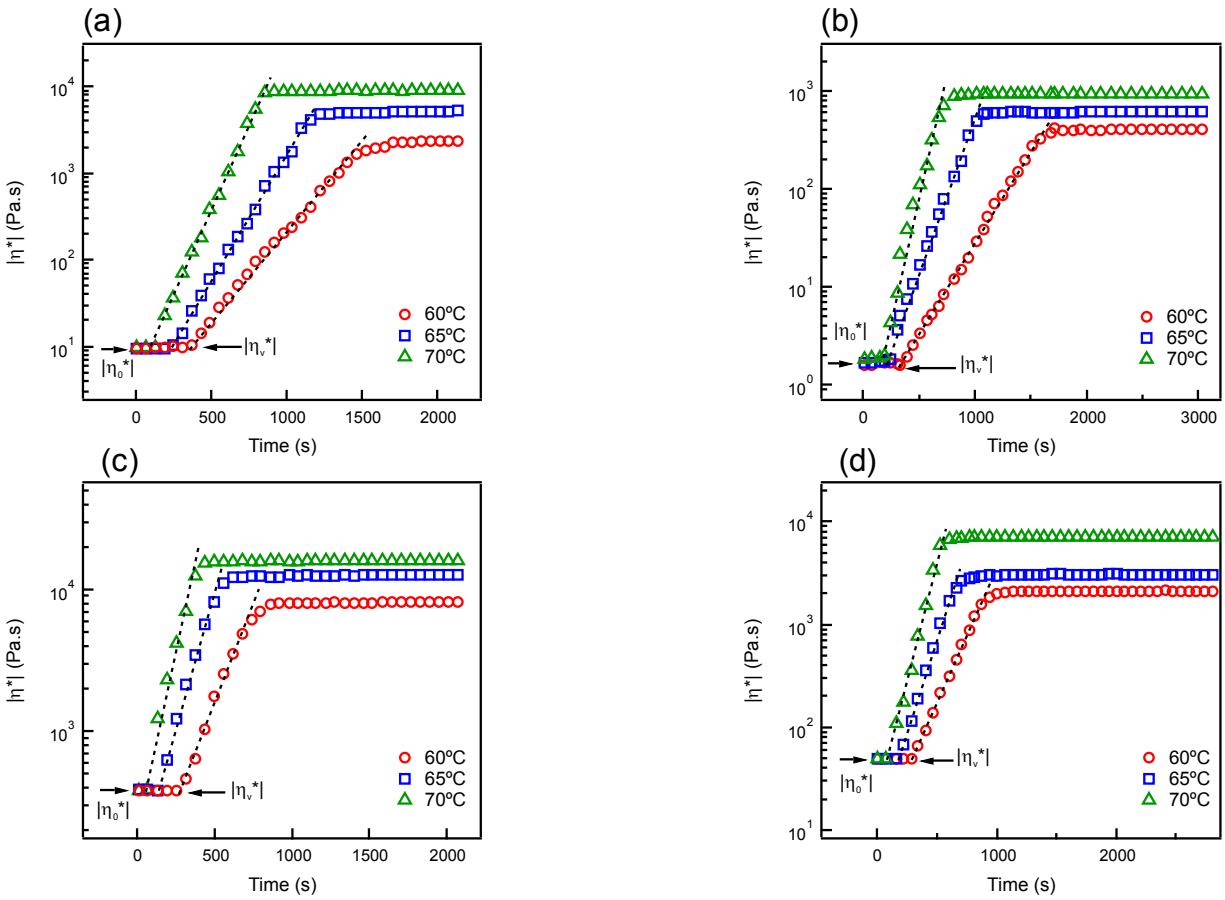

Figure 8. Evolution of complex viscosity at different curing temperatures for (a) P84-L_α, (b) L121-L_α, (c) P84-H_2, and (d) L64-H_2 samples. The dashed lines show the fitted slope in the propagation step.

From Figure 7, the initial complex viscosity of the mesophase samples, shown by an arrow in the graphs, does not change with temperature, which can be attributed to the confined structure of LLCs that hinders the free movement. Therefore, thermal dependency of their viscosity is negligible ($E_v = 0$). The polymerization stage of $|\eta^*|$ versus time is fitted with eq. (10) and the model parameters are summarized in Table 2. Refer to Figure 6b for the bulk data. The polymerization rate in the reverse hexagonal confinement is higher than that of the lamellar ones. We believe the degree of confinement [2,20] contributes to the higher polymerization rate in the reverse hexagonal mesophases.

As discussed in the introduction, the degree of confinement can be related to the elastic modulus [65,66] and the domain size [67,68] of confinement. From the rheological data, the reverse hexagonal mesophases have higher elastic modulus compared to the lamellar ones. Therefore, according to eq. (1) we ideally expect to see a smaller change in the domain size of H_2 samples upon polymerization than the L_α ones. However, analysis of SAXS results in Table 2 shows that the P84-H_2 mesophase has a higher change in domain size upon polymerization compared to the P84-L_α sample. Deviation from eq. (1) can be attributed to dynamic changes in the interfacial properties of the mesophases and shows that factors other than elastic modulus are responsible for the change in domain size. The change in domain size results show that the stiffness contribution to degree of confinement is lower for reverse hexagonal mesophases than the lamellar ones.

Additionally, as shown in Figure 3, the size of confinement in the reverse hexagonal and lamellar systems can be calculated from the radius of the biggest circle ($R_{h,\,max}$ and $R_{l,\,max}$) that can be contained in the apolar domain (the bigger the sphere, the bigger is the confinement size). The radius of such circle is equal to the half of the monomeric domain size in the lamellar samples, as:

$$R_{l,\,max} = \frac{D_1}{2} \tag{12}$$

whereas for reverse hexagonal mesophases, $R_{h,\,max}$ is obtained as follows:

$$R_{h,\,max} = \sqrt{\frac{A_h}{\pi}} \tag{13a}$$

$$A_h = \frac{a^2\sqrt{3}}{4} - \frac{\pi(M_H)^2}{2} \tag{13b}$$

Parameters are schematically shown in Figure 3. Confinement sizes are calculated for all samples based on the SAXS data and reported in Table 2 (detailed calculations are provided in the ESI). We observe that for the same polymerizing chain, the lamellar mesophases provide a smaller confinement size, compared to the hexagonal ones. Therefore, by considering both size and stiffness contributions to the confinement, we conclude that the P84- H_2 has the lowest degree of confinement and the P84- L_α has the highest one.

Our results in Table 2 show that the polymerization rate decreases with increasing the degree of confinement. In the confined structures, the probability of two macroradicals to react with each other increases that leads to a higher termination rate. Therefore, the rate of polymerization as well as the conversion decrease.[15] In fact, we can consider the mesophase polymerization similar to the polymerizations of a dispersed phase in miniemulsions and emulsions. In such systems, the concentration of radicals in the dispersed phase varies depending on the volume of the monomer droplets/polymer particles dispersed in the continuous phase.[69,70] In this work, rather than being confined inside droplets of a dispersed phase, the reaction is confined within the structures of the lamellar and reverse hexagonal mesophases. Salsamendi and coworkers have considered the confinement effects experienced by propagating radicals to explain the significantly reduced rate of polymerization.[71] They developed a mathematical model to take into account the segregation effects on the polymerization rate. Their segregation model predicts that bulk free radical polymerization would proceed at a much faster rate compared to nanoconfined structures. Our data show that the polymerization proceeds significantly faster in the bulk state compared to the reverse hexagonal and lamellar samples. The lamellar systems have the slowest polymerization rates. Therefore, our results are in agreement with the segregation model, which predicts that as the degree of confinement increases, the probability of the termination increases due to the higher local radical concentration resulting in a slower rate of polymerization.[71] Comparing the polymerization rates of two hexagonal samples together (and likewise the two lamellar ones together) suggests that the major contribution to the degree of confinement comes from the size rather than modulus/change in domain size.

Chemorheology results show that final values of dynamic moduli increase with curing temperature (Figure 5). Mechanical properties of the crosslinked polymer control the elastic modulus of each sample that in turn is proportional to the reaction conversion. In order to confirm this hypothesis, the conversion of the samples cured at different temperatures is measured using the gravimetric technique and plotted against curing temperature (Figure 9). After the polymerization is ended, we measured the rheological properties of each cured sample at different temperatures to investigate the temperature dependency of the final elastic modulus (data shown in Figure S10 of the ESI). We found

that the elastic modulus of polymerized samples decreases with increasing temperature from 25 to 70 °C, because the polymer network becomes softer by increasing the temperature. In addition, according to poroelasticity theory, the decrease in elastic modulus of polymerized mesophases could be due to the decrease in the water viscosity by temperature.[72,73] Final elastic modulus of the samples, all measured at 70 °C (to remove the effect of temperature), are plotted against the conversion in Figure 9b. The results suggest that G'_{final} is linearly correlated with the reaction conversion within the studied range of temperature. The enhanced conversion with raising curing temperature is attributed to the increase in polymerization rate and monomer diffusion coefficients.[33]

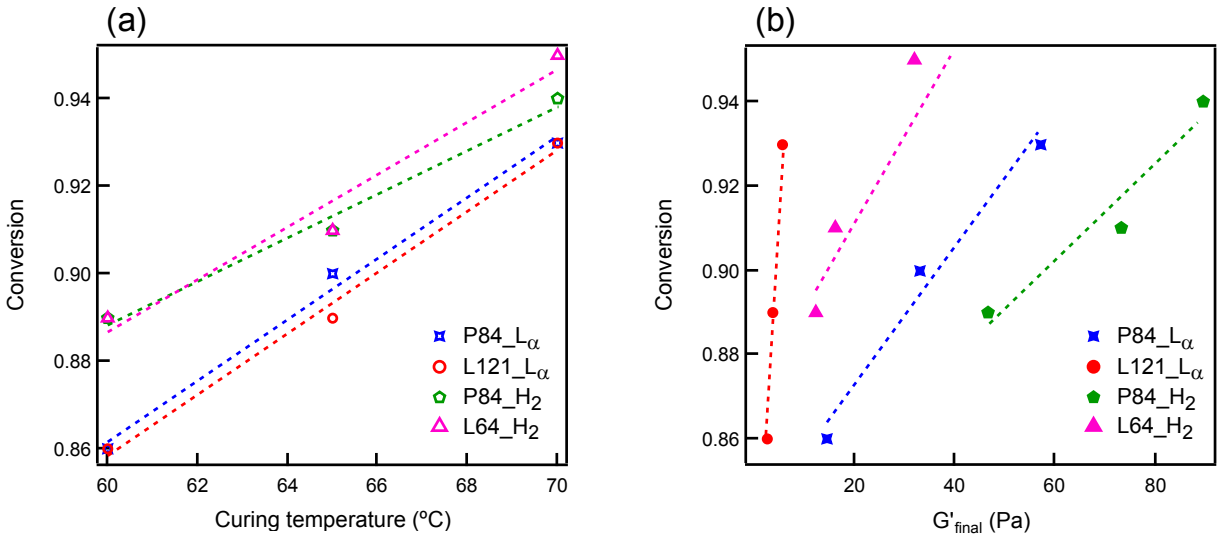

Figure 9. (a) Effect of curing temperature on conversion of each mesophase system. (b) The conversion against the storage modulus of cured samples measured at 70 °C.

DSC Measurements

To confirm the kinetic parameters obtained from chemorheological studies, DSC is performed on two typical samples with lamellar and hexagonal structures (P84-L_α and P84-H_2). The polymerization rate versus time (Figure 10) and conversion versus time plots (Figure 11) confirm that the radical polymerization in mesophases is influenced by the diffusion-controlled phenomena.

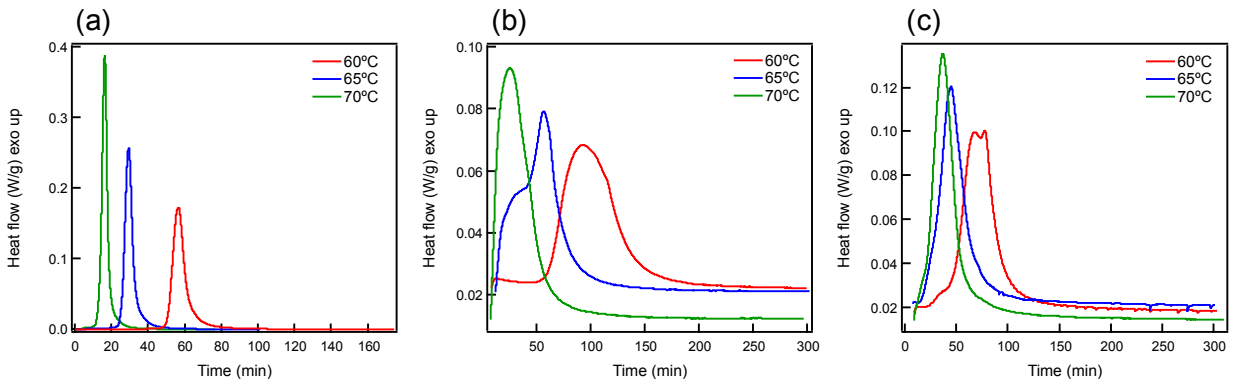

Figure 10. The effect of temperature on the variation of heat flow with time during isothermal polymerization of (a) bulk, (b) P84-L$_\alpha$, and (c) P84-H$_2$.

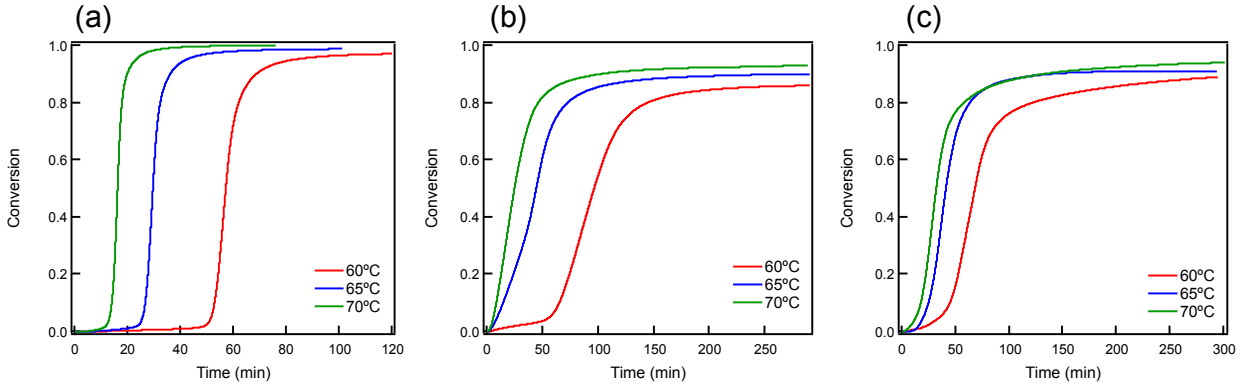

Figure 11. The effect of temperature on the variation of conversion with time during isothermal polymerization of (a) bulk, (b) P84-L$_\alpha$, and (c) P84-H$_2$.

In the first stage of polymerization (low conversions), an almost linear dependence of conversion, and an approximately constant R_p appears, indicating purely chemical-controlled nature of the polymerization.[74] In the region of 10-20 % conversion, a sharp increase in the reaction rate (autoacceleration) starts followed by an increase in the conversion values.[75,76] The autoacceleration (gel effect) is attributed to the effect of diffusion-controlled phenomena on the termination reaction.

By considering the steady-state hypothesis for the free radical concentration, the polymerization rate, R_p, is given as a function of conversion, X:[76]

$$\frac{R_p}{[M]} = \frac{dX}{dt} = k_p\left(\frac{fk_d}{k_t}\right)^{1/2}[I]^{1/2}(1-X) \cong K'(1-X) \qquad (14a)$$

$$K' = k_p\left(\frac{fk_d}{k_t}\right)^{1/2}[I]^{1/2} \quad (14b)$$

where k_d represents the kinetic rate constant of initiator decomposition and f is the initiator efficiency. The propagation and termination rate constants are k_p and k_d, respectively.

To investigate the effect of temperature on the reaction kinetics, equation (14a) can be integrated by considering that all the kinetic rate coefficients, initiator concentration, and efficiency are constant. Therefore, an expression which directly correlates the monomer conversion with an observed overall kinetic rate coefficient, K', will be obtained:

$$-ln(1-X) = K't \quad (15)$$

It should be noted that mentioned assumptions are valid only for the low degrees of monomer conversion.[76] The slope of the initial linear part (between 2 to 10 % where autoacceleration is negligible) of the plot of $-ln(1-X)$ versus t, gives the overall kinetic rate constant.[16,76] Accordingly, the overall kinetic rate values are measured at different temperatures for the bulk state and two typical samples with lamellar and hexagonal structures. The overall activation energy of polymerization is obtained by considering an Arrhenius type dependency of reaction rate to temperature.

Table 3 shows the kinetic parameters derived from DSC. As seen, the polymerization rate in nanoconfined structures is significantly (one order of magnitude) lower than that of the bulk polymerization which is in agreement with chemorheology results. As mentioned earlier, the DSC results (Figure 10 and 11) show that the radical polymerization in mesophases is controlled by the diffusion-controlled phenomena. The activation energies obtained from chemorheology (Table 2) and DSC (Table 3) experiments show that the reverse hexagonal mesophases have higher activation energy than lamellar ones (bulk has the lowest activation energy). This is attributed to the higher viscosity of the reverse hexagonal systems compared to the lamellar samples at the early stages of polymerization. On the other hand, it is observed that by increasing the degree of confinement in the system the gel effect decreases during the polymerization. It is confirmed that the lamellar mesophase with the highest degree of confinement has the

lowest conversion (Figure 9) and polymerization rate, which are induced by the increase in the termination rate.

These results show that the confinement effect is competing with the gel effect when the polymerization is proceeding within the mesophase system. The high degree of confinement increases the probability of two radicals to react with each other and consequently increases the termination rate.

Table 3. Activation energy and kinetic rate constants of polymerization for bulk and confined structures at different temperatures derived from DSC measurements.

Sample	E (kJ/mol)	K' (10^{-3}/s) (60 °C)	K' (10^{-3}/s) (65 °C)	K' (10^{-3}/s) (70 °C)
P84- H_2	84	3.6	8.5	9.1
P84- L_α	75	3.4	7.6	8.2
Bulk polymerization	52	21.4	25.3	37.3

Conclusion

In this paper, we described a detailed analysis of the thermal polymerization kinetics of monomers in ternary lyotropic liquid crystal systems. The degree of confinement in these systems is controlled by the confinement size and the stiffens of the template. The stiffness can be measured by the elastic modulus or change in domain size upon polymerization, which are inversely proportional except if the properties of the template change during polymerization. We discussed that the reverse hexagonal structures offer less degree of confinement than the lamellar samples. Three stages of polymerization (i.e., induction, polymerization and final curing) were observed in the chemorheology. We found that the viscosity of the mesophases contributes to the initial and total activation energy of the polymerization. The results from the chemorheology and DSC also showed that the rate of polymerization decreases significantly in confined structures compared to the bulk polymerization. Additionally, the polymerization rate was higher in reverse hexagonal mesophases than that of the lamellar structures. This phenomenon was

attributed to the segregation effects in which as the degree of confinement increases, the probability of the termination increases due to the higher local radical concentration. At the final stages of the polymerization, a lower limiting conversion was observed in the lamellar systems compared to the reverse hexagonal ones, because the higher degree of confinement in the lamellar mesophases leads to a higher rate of termination in the late stages of polymerization.

Acknowledgement

The authors thank Aaron Lindsay for assistance with SAXS measurements. This work was supported by the U.S. Department of Interior, Bureau of Reclamation (Agreement No. R10AC80283). This work was performed in part at the Center for Integrated Nanotechnologies (CINT). CINT is funded by the DOE Office of Basic Energy Sciences. LANL is operated by Los Alamos National Security, LLC, for the National Nuclear Security Administration of the U.S. Department of Energy under contract DE-AC52-06NA25396. Financial support from National Science Foundation (award No. 1438584) is gratefully acknowledged.

References

1 B. S. Forney and C. A. Guymon, *Macromolecules*, 2010, **43**, 8502–8510.

2 C. L. Lester, C. D. Colson and C. A. Guymon, *Macromolecules*, 2001, **34**, 4430–4438.

3 W. Srisiri, T. M. Sisson, D. F. O'Brien, K. M. McGrath, Y. Han and S. M. Gruner, *J. Am. Chem. Soc.*, 1997, **119**, 4866–4873.

4 C. T. Kresge, M. E. Leonowicz, W. J. Roth, J. C. Vartuli and J. S. Beck, *Nature*, 1992, **359**, 710–712.

5 J. S. Beck, J. C. Vartuli, W. J. Roth, M. E. Leonowicz, C. T. Kresge, K. D. Schmitt, C. T. W. Chu, D. H. Olson and E. W. Sheppard, *J. Am. Chem. Soc.*, 1992, **114**, 10834–10843.

6 P. Feng, X. Bu and D. J. Pine, *Langmuir*, 2000, **16**, 5304–5310.

7 S. Grubjesic, B. Lee, S. Seifert and M. A. Firestone, *Soft Matter*, 2011, **7**, 9695.

8 K. S. Worthington, C. Baguenard, B. S. Forney and C. A. Guymon, *J. Polym. Sci. Part B Polym. Phys.*, 2017, **55**, 471–489.

9 L. Sievens-Figueroa and A. Guymon, *Macromolecules*, 2009, **42**, 9243–9250.

10 M. A. DePierro, K. G. Carpenter and C. A. Guymon, *Chem. Mater.*, 2006, **18**, 5609–5617.

11 J. Zhang, Z. Xie, M. Hoang, A. J. Hill, W. Cong, F. H. She, W. Gao and L. X. Kong, *Soft Matter*, 2014, **10**, 5192–5200.

12 J. Zhang, Z. Xie, A. J. Hill, F. H. She, A. W. Thornton, M. Hoang and L. X. Kong, *Soft Matter*, 2012, **8**, 2087–2094.

13 C. C. Co, *Soft Matter*, 2008, **4**, 658.

14 N. Massad-Ivanir, T. Friedman, A. Nahor, S. Eichler, L. M. Bonanno, A. Sa'ar and E. Segal, *Soft Matter*, 2012, **8**, 9166.

15 B. Sanz, N. Ballard, J. M. Asua and C. Mijangos, *Macromolecules*, 2017, **50**, 811–821.

16 H. Zhao and S. L. Simon, *Polymer (Guildf).*, 2011, **52**, 4093–4098.

17 S. Alexandris, P. Papadopoulos, G. Sakellariou, M. Steinhart, H.-J. Butt and G. Floudas, *Macromolecules*, 2016, **49**, 7400–7414.

18 C. Mijangos, R. Hernández and J. Martín, *Prog. Polym. Sci.*, 2016, **54**–**55**, 148–182.

19 Y. Suzuki, H. Duran, M. Steinhart, H.-J. Butt and G. Floudas, *Soft Matter*, 2013, **9**, 2621.

20 M. A. DePierro and C. A. Guymon, *Macromolecules*, 2014, **47**, 5728–5738.

21 J. D. Clapper, L. Sievens-Figueroa and C. A. Guymon, *Chem. Mater.*, 2008, **20**, 768–781.

22 M. A. DePierro and C. A. Guymon, *Macromolecules*, 2006, **39**, 617–626.

23 L. C. Lester and C. A. Guymon, *Macromolecules*, 2000, **33**, 5448–5454.

24 P. Alexandridis, U. Olsson and B. Lindman, *J. Phys. Chem.*, 1996, **100**, 280–288.

25 P. Alexandridis, U. Olsson and B. Lindman, *Langmuir*, 1998, **14**, 2627–2638.

26 P. Holmqvist, P. Alexandridis and B. Lindman, *Langmuir*, 1997, **13**, 2471–2479.

27 P. Alexandridis and B. Lindman, *Amphiphilic Block Copolymers: Self-assembly and Application*, Elsevier, 2000.

28 D. T. McCormick, K. D. Stovall and C. A. Guymon, *Macromolecules*, 2003, **36**, 6549–6558.

29 C. L. Lester, S. M. Smith and A. Guymon, *Macromolecules*, 2001, **34**, 8587–8589.

30 L. Silies, H. Didzoleit, C. Hess, B. Stü and A. Andrieu-Brunsen, *Chem. Mater.*, 2015, **27**, 1971–1981.

31 M. Antonietti, C. Göltner and H.-P. Hentze, *Langmuir*, 1998, **14**, 2670–2676.

32 H.-P. Hentze and E. W. Kaler, *Curr. Opin. Colloid Interface Sci.*, 2003, **8**, 164–178.

33 R. Foudazi, P. Gokun, D. L. Feke, S. J. Rowan and I. Manas-Zloczower, *Macromolecules*, 2013, **46**, 5393–5396.

34 B. Strachota, L. Matějka, A. Sikora, J. Spěváček, R. Konefał, A. Zhigunov, M. Šlouf and L. Matějka, *Soft Matter*, 2017, **13**, 1244–1256.

35 C. A., S. K., S.-M. J. F. A., W. Q., P. J. A. and M.-M. J. D., *RSC Adv.*, 2016, **6**, 81694–81702.

36 M. Di Biase, P. de Leonardis, V. Castelletto, I. W. Hamley, B. Derby and N. Tirelli, *Soft Matter*, 2011, **7**, 4928.

37 S. Peng, P. G. Hartley, T. C. Hughes, Q. Guo, M. Y. Guo, S. B. Wei, S. L. Qiu, R. H. Templer, T. H. Nguyen, T. M. Hinton, L. J. Waddington, N. Kirby, D. K. Wright, H. X. Wang, G. E. Egan and B. A. Moffat, *Soft Matter*, 2015, **11**, 6318–6326.

38 A. W. Chow, J. F. Sandell and J. F. Wolfe, *Polymer (Guildf).*, 1988, **29**, 1307–1312.

39 A. W. Chow, R. D. Hamlin, J. F. Sandell and J. F. Wolfe, *MRS Proc.*, 1988, **134**, 95.

40 S. Qavi, A. P. Lindsay, M. A. Firestone and R. Foudazi, *J. Memb. Sci.*, 2019, **580**, 125–133.

41 G. Odian, *Principles of Polymerization*, John Wiley & Sons, 2004.

42 P. Alexandridis, U. Olsson and B. Lindman, *Macromolecules*, 1995, **28**, 7700–7710.

43 S. Qavi, M. A. Firestone and R. Foudazi, *Soft Matter*, 2019, **15**, 5626–5637.

44 B. A. Smith, E. T. Samulski, L.-P. Yu and M. A. Winnik, *Phys. Rev. Lett.*, 1984, **52**, 45–48.

45 A. K. Fritzsche and F. P. Price, *Polym. Eng. Sci.*, 1974, **14**, 401–412.

46 N. Ileri Ercan, P. Stroeve, J. W. Tringe and R. Faller, *Langmuir*, 2016, **32**, 10026–10033.

47 K. Bryskhe, K. Schillen, J.-E. Lofroth and U. Olsson, *Phys. Chem. Chem. Phys.*, 2001, **3**, 1303–1309.

48 R. Foudazi, S. Qavi, I. Masalova and A. Y. A. Y. Malkin, *Adv. Colloid Interface Sci.*, 2015, **220**, 78–91.

49 K. Hyun, J. G. Nam, M. Wilhellm, K. H. Ahn and S. J. Lee, *Rheol. Acta*, 2006, **45**, 239–249.

50 S. R. Raghavan and S. A. Khan, *J. Colloid Interface Sci.*, 1997, **185**, 57–67.

51 C. Bower, C. Gallegos, M. R. Mackley and J. M. Madiedo, *Rheol. Acta*, 1999, **38**, 145–159.

52 J. Zipfel, J. Berghausen, G. Schmidt, P. Lindner, P. Alexandridis, M. Tsianou and W. Richtering, *Phys. Chem. Chem. Phys.*, 1999, **1**, 3905–3910.

53 J.-P. Habas, E. Pavie, A. Lapp and J. Peyrelasse, *Rheol. Acta*, 2008, **47**, 765–776.

54 J. N. Israelachvili, *Intermolecular and Surface Forces*, Academic Press, third edit., 1992.

55 R. Foudazi, I. Masalova and A. Y. Malkin, *J. Rheol. (N. Y. N. Y).*, 2012, **56**, 1299–1314.

56 T. Mason, J. Bibette and D. Weitz, *Phys. Rev. Lett.*, 1995, **75**, 2051–2054.

57 R. J. Ketz, R. K. Prud'homme and W. W. Graessley, *Rheol. Acta*, 1988, **27**, 531–539.

58 M. Laurati, G. Petekidis, N. Koumakis, F. Cardinaux, A. B. Schofield, J. M. Brader, M. Fuchs and S. U. Egelhaaf, *J. Chem. Phys.*, 2009, **130**, 134907(1-14).

59 P. Sollich, *Phys. Rev. E*, 1998, **58**, 738–759.

60 S. Qavi and R. Foudazi, *Rheol. Acta*, 2019, **58**, 483–498.

61 P. J. Flory, *Principles of Polymer Chemistry*, Cornell University Press, 1953.

62 H. H. Winter and F. Chambon, *J. Rheol. (N. Y. N. Y).*, 1986, **30**, 367–382.

63 A. Y. Malkin and S. G. Kulichikhin, *Polymer Compositions Stabilizers/Curing SE-5*, Springer-Verlag, Berlin/Heidelberg, 1991, vol. 101.

64 P. J. Halley and M. E. Mackay, *Polym. Eng. Sci.*, 1996, **36**, 593–609.

65 I. Koltover, T. Salditt, J. O. Rädler and C. R. Safinya, *Sci.* , 1998, **281**, 78–81.

66 V. Allain, C. Bourgaux and P. Couvreur, *Nucleic Acids Res.*, 2012, **40**, 1891–1903.

67 Y. Li, O. S. Sarıyer, A. Ramachandran, S. Panyukov, M. Rubinstein and E. Kumacheva, *Sci. Rep.*, 2015, **5**, 17017.

68 B. Yu, P. Sun, T. Chen, Q. Jin, D. Ding, B. Li and A.-C. Shi, *Phys. Rev. Lett.*, 2006, **96**, 138306.

69 C. Autran, J. C. de la Cal and J. M. Asua, *Macromolecules*, 2007, **40**, 6233–6238.

70 T. G. T. Jansen, J. Meuldijk, P. A. Lovell and A. M. van Herk, *J. Polym. Sci. Part A Polym. Chem.*, 2016, **54**, 2731–2745.

71 M. Salsamendi, N. Ballard, B. Sanz, J. M. Asua and C. Mijangos, *RSC Adv.*, 2015, **5**, 19220–19228.

72 J. Dvorkin, R. Nolen-Hoeksema and A. Nur, *Geophysics*, 1994, **59**, 428–438.

73 E. Detournay and A. H. Cheng, 1993, **II**, 113–171.

74 D. S. Achilias, *Macromol. theory simulations*, 2007, **16**, 319–347.

75 P. Siafaka and D. S. Achilias, *Macromol. Symp.*, 2013, **331–332**, 166–172.

76 D. S. Achilias, *J. Therm. Anal. Calorim.*, 2014, **116**, 1379–1386.

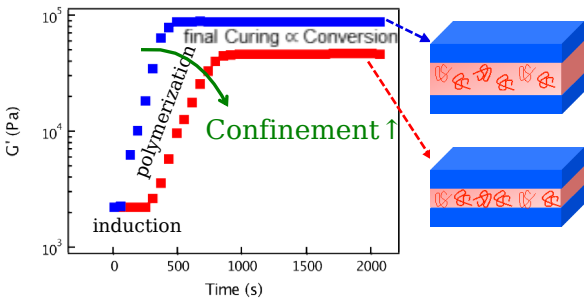
final Curing ∝ Conversion
polymerization
Confinement ↑
induction
G' (Pa)
Time (s)
10^5
10^4
10^3
0
500
1000
1500
2000